Human Welder 3-D Hand Movement Learning in Virtualized GTAW: Theory and Experiments

Yukang Liu and Yuming Zhang

Abstract Combining human welder (with intelligence and sensing versatility) and automated welding systems (with precision and consistency) can lead to next generation intelligent welding systems. This paper aims to present a data-driven approach to model human welder hand movement in 3-D, and use the learned model to control automated Gas Tungsten Arc Welding (GTAW) process. To this end, an innovative virtualized welding platform is utilized to conduct teleoperated training experiments: the welding current is randomly changed to generate fluctuating weld pool surface and a human welder tries to adjust the torch movements in 3-D (including welding speed, arc length, and torch orientations) based on the observation on the real-time weld pool image feedback. These torch movements together with the 3-D weld pool characteristic parameters are recorded. The weld pool and human hand movement data are off-line rated by the welder and a welder rating system is trained, using an Adaptive Neuro-Fuzzy Inference System (ANFIS), to automate the rating. Data from the training experiments are then automatically rated such that top rated data pairs are selected to model and extract "good response" minimizing the effect from "bad operation" made during the training. ANFIS model is then utilized to correlate the 3-D weld pool characteristic parameters and welder's torch movements. To demonstrate the effectiveness of the proposed model as an effective intelligent controller, automated control experiments are conducted. Experimental results verified that the controller is effective under different welding currents and is robust against welding speed and measurement disturbances. A foundation is thus established to learn human welder intelligence, and transfer such knowledge to realize intelligent welding robot.

Keywords Welder intelligence learning · ANFIS · Welder rating system
Virtualized welding · GTAW

Y. Liu (✉) · Y. Zhang
Institute for Sustainable Manufacturing and Department of Electrical and Computer Engineering, University of Kentucky, Lexington, KY 40506, USA
e-mail: webberliu@gmail.com

S. Chen et al. (eds.), *Transactions on Intelligent Welding Manufacturing*,
Transactions on Intelligent Welding Manufacturing,
https://doi.org/10.1007/978-981-10-8740-0_1

1 Introduction

GAS Tungsten Arc Welding (GTAW) is the primary process used for precision joining of metals [1]. In this process (shown in Fig. 1) an arc is established between the non-consumable tungsten electrode and the base metal. The base metal is melted by the arc forming a liquid weld pool that joins the two pieces of base metal together after solidification. The shielding gas is fed through the torch to protect the electrode, molten weld pool, and solidifying weld metal which may be contaminated by the surrounding atmosphere. Automated GTAW systems may produce repeatable results by accurately controlling the joint fit-up and welding conditions to reduce possible process variations but at high costs while the resultant weld quality may still not always be assured. Welding process monitoring and control for automated welding machines thus have been extensively studied in the past few decades [2–10]. Various sensing and control techniques have been proposed, including pool oscillation [2, 3], radiography [4, 5], thermal [6, 7], and vision [8–10] based sensing and control. In particular, the weld pool geometry is believed to provide valuable insights into the state of the welding process. Important information such as weld defects and weld joint penetration are contained in the surface deformation of the weld pool [10]. Recently an innovative vision-based 3-D weld pool sensing system for GTAW process was developed in the Welding Lab at University of Kentucky [11]. The weld pool was further characterized by its width, length and convexity instead of a large set of 3-D coordinates. The weld penetration and weld pool surface have thus been accurately controlled [9, 10, 12]. To ensure such an ideal closed-loop control performance, however, the control algorithm (structure) needs to be carefully designed per the process dynamics. The ability to develop an appropriate control algorithm requires control system design experience and solid understanding of process dynamics.

Besides conventional modeling and control methodology based on welding process inputs/outputs, human welder intelligence based modeling and control [13]

Fig. 1 Illustration of GTAW

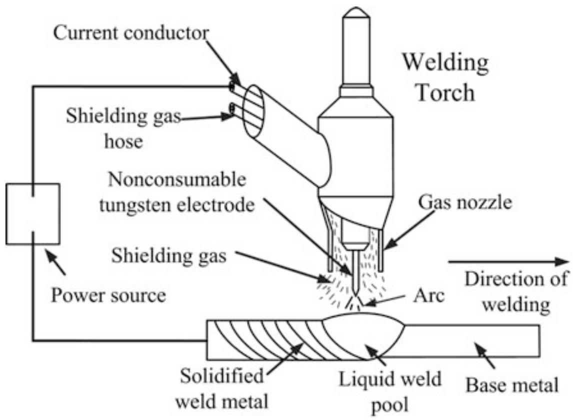

provides an alternative route to develop welding process control algorithms. It is inspired by the fact that in manual GTAW process human welders can appraise the welding process based on their observations on the welding process to adjust welding parameters to adaptively overcome the effects due to variations in the welding conditions. Learning human welder response and transferring such intelligence to the welding robot thus would provide a convenient method to take advantage of valuable human welder experience and utilize the accurate execution of the robot to exceed human physical limitations [14, 15]. The resultant intelligent welding robots may also help resolve the skilled welder shortage issue the manufacturing industry is currently facing [16]. Moreover, the design of the control algorithm becomes a one step process—modeling human welder's response as function of feedback from the sensor. The design thus becomes simpler and less designer dependent.

The main welding parameters in GTAW that human welders tend to control include welding current and speed, arc length, and torch orientations, etc. Both welding current and speed can significantly affect the heat input into the welding process and thus influencing the weld pool surface geometry and weld penetration considerably [10]. Arc length also has certain impact on welding arc's penetration capabilities. Because the welding current in GTAW is controlled by the constant current power supply, an increase in the arc length results in an increase in the arc voltage and arc power. However, the distribution of the arc energy is decentralized such that the efficiency of the arc and the penetration capability might decrease consequently. Torch orientations are also considered to be correlated to the weld quality and appearance. Inappropriate torch manipulations may cause weld defects including undercut, porosity, and cracks. In [13–15], welding current has been controlled where the pipe rotates and the torch is always on 12 o'clock (i.e., 1G welding position). However, in many pipe welding applications the pipe stays stationary during welding and the welding torch moves along the weld joint (i.e., 5G welding position) [17, 18]. In this case welders choose a pre-defined welding current and move the torch along the pipe. The movements of the torch (i.e. the welding speed, arc length, and torch orientations) are thus controlled by the human welder as main sources to compensate for possible process variations. Different control algorithms have been proposed to control the welding process by adjusting the welding speed, either through traditional system identification/controller design approach [19], through directly modeling human welder response [20, 21], or a combination of the two approaches [22]. Although these algorithms have demonstrated certain success in controlling the welding process by adjusting the welding speed, the limitation of the single input (i.e., welding speed) needs to be relaxed. Actually, in manual GTAW process, the human welder can perform welding operations freely in 3-D space. It indicates that for an intelligent welding robot that can mimic or even outperform human welder, it should be able to control the welding process by operating the welding torch freely in 3-D space. The key challenge in learning human welder decision making for intelligent welding robot development thus lies in the availability of such unique ability that allows the human welder to perform naturally and freely in 3D space while still can monitor the inputs (weld pool surface) and outputs (adjustments on welding parameters) of the decision process [23].

This paper utilizes a recently developed virtualized welding platform [24, 25] to perform welder teleoperation experiments, proposes an ANFIS based data-driven approach to model the human welder's adjustments in 3-D, and transfers this model to the welding robot to perform automated welding. The remainder of the paper is organized as follows. In Sect. 2 experimental system is described and human motion is analyzed. In Sect. 3 training experiments are conducted in which human welder adjustments together with 3-D weld pool characteristic parameters are recorded. The experimental data are also presented in this section. An automated welder rating system is trained in Sect. 4, and "good responses" are selected. Linear model and ANFIS model are used to correlate the torch movements and the weld pool characteristic parameters in Sect. 5. To verify the robustness of the proposed intelligent model, automated welding experiments under varying welding currents and speed disturbance are conducted and the results are analyzed in Sect. 6. Conclusions are finally drawn in Sect. 7.

2 Experimental System and Human Hand Motion Analysis

2.1 Experimental System Set-Up

In this subsection the teleoperation based virtualized welding platform is briefly introduced. This system is illustrated in Fig. 2a together with the experimental setup [24]. It consists of two workstations: welding station and virtual station. In virtual station a human welder can view the mock up where the weld pool image feedback is displayed and moves the virtual welding torch accordingly as if he/she is right in front of the work-piece. The human welder movement is accurately

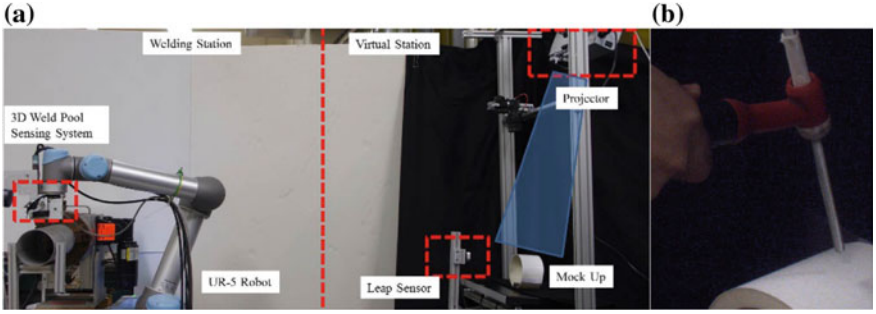

Fig. 2 **a** General view of the virtualized welding system; **b** virtual welding torch

captured by a Leap motion sensor, and the obtained virtual welding torch (Fig. 2b) 3-D coordinates and orientations will be sent to the PC. Leap sensor is an advanced motion sensor which is utilized in this study to accurately capture the human welder's adjustments on torch movement. It can track fingers or similar items to a spatial precision of 0.01 mm [26].

The welding station consists of an industrial welding robot, stainless steel pipe, and a compact 3-D weld pool sensing system [24]. The robot utilized in this study is Universal Robot UR-5 with six Degree of Freedom. The robot arm equipped with the welding torch receives commands (next robot tool pose including robot tool 3-D positions and orientations) via Ethernet from the PC, executes the command and sends the current robot tool position back to the PC. Figure 3 depicts a detailed view of the 3-D weld pool sensing system as well as weld pool characteristic parameters [11]. Camera 2 (eye view camera) captures the weld pool image and sent it back to the PC (a sample image is shown in lower left). A low power laser (19 by 19 structure light pattern) is projected to the weld pool surface and its reflection from the specular weld pool surface is intercepted by an imaging plane and imaged by a CCD camera (Camera 1 in Fig. 3a). It is known that arc light is an omni-directional light source. Its intensity decreases quadratically with the distance traveled, but the laser, due to its coherent nature, does not significantly lose its intensity. Hence, it is possible to intercept the reflection of the illumination laser from the weld pool surface with an imaging plane placed at an appropriate distance from the arc. From the distorted reflection pattern on the imaging plane and the assumption of a smooth weld pool surface, the 3-D shape of the weld pool surface can be obtained. By using specific image processing and reconstruction algorithms [11], 3-D specular weld pool can be reconstructed in real-time (a sample reconstructed weld pool is shown in lower right).

2.2 Human Hand Motion Analysis

Human hand motion consists of both deterministic and stochastic movement. By utilizing the leap motion sensor, fine human hand movement can be accurately detected and recorded. However, it is not clear when the teleoperation training experiments are conducted, what types of human hand motion should be followed by the robot. If the stochastic and high frequency human hand tremor or large movement is transferred to the robot, the robot tracking performance cannot be guaranteed.

To analyze the human hand motion, ten experiments are conducted where human welder moves the virtual welding torch along the mock-up pipe, and his/her movement is recorded by the leap sensor. Figure 4 depicts human hand motion in a sample experiment. It is seen that human moves the virtual welding torch along x axis (i.e., welding direction), from −20 to 20 mm (corresponding to about −20° to 20° relative to the vertical direction). Sudden movements along z axis (i.e., arc length) are also observed. For example, from 42 to 43 s, movement along z axis

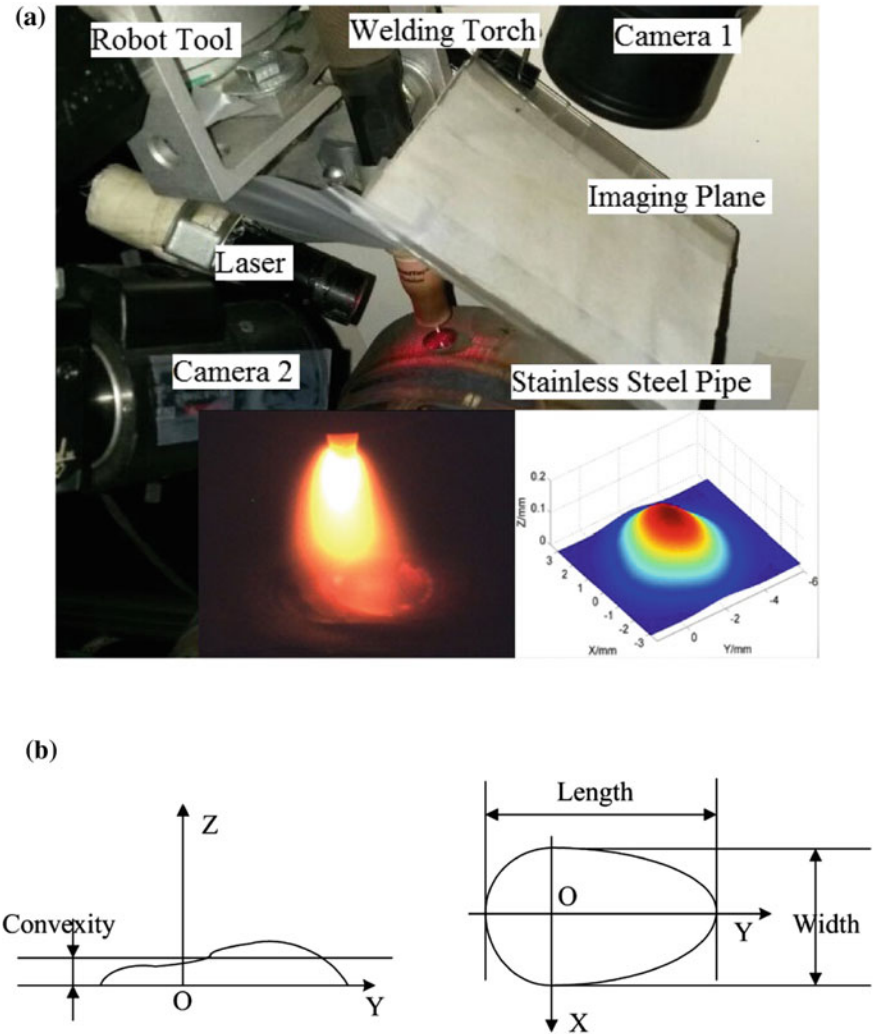

Fig. 3 **a** Detailed view of the 3D weld pool sensing system; **b** weld pool characteristic parameters

fluctuates between −8 and 8 mm. This type of movement is considered as noise and should not be followed by the robot. Movement along y axis (perpendicular to the welding direction) should be following the shape of the weld seam. For our application which is pipe welding along a straight line, y coordinate should keep constant (0 mm in this study). However, from Fig. 4 it is observed that y coordinates vary from −2 to 3 mm. This is expected because the human welder movement includes the stochastic part, thus can't be accurately controlled like the welding robot. *RX* movement, i.e., rotation along the welding direction ranges from −4° to 6° in this sample experiment. For automated welding machines, *RX* is normally kept

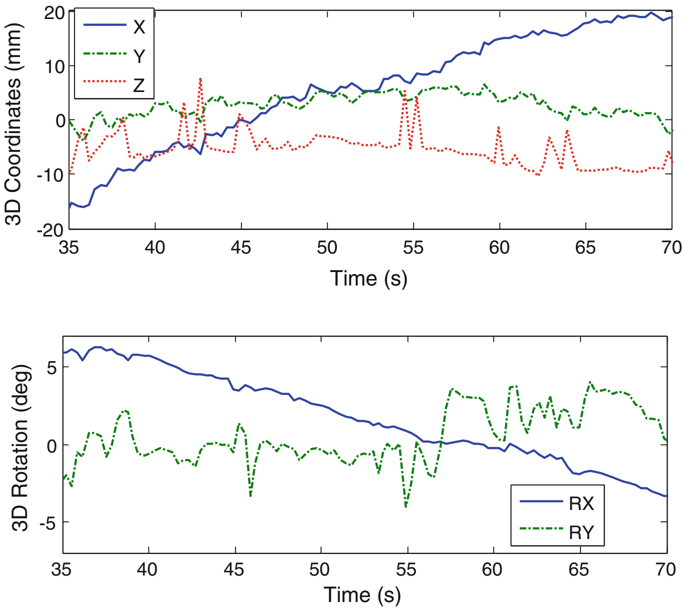

Fig. 4 Sample human hand motion captured by leap sensor for movement along the pipe

perpendicular to the pipe surface. For manual welding process, however, this rotation along the welding direction is controlled by the human welder. *RY*, i.e., rotation perpendicular to the welding direction, ranges from $-4°$ to $4°$ with certain fluctuations. *RZ*, or rotation along the welding torch, does not affect the welding performance and is thus not considered in this study. To summarize, four human movements are considered: *X*, *Z*, *RX*, *RY*, which correspond to the welding speed, arc length, orientation along and perpendicular to welding direction, respectively. Figure 5 plots the histograms for these four movements in ten experiments. Figure 6 depicts the Power Spectral Density (PSD) in these experiments. It is observed that coordinate and orientation along welding direction (*X* and *RX*) have smaller variation in PSD than *Z* and *RY* movements. The following low-pass filter is proposed to filter the human hand motion:

$$m_{i,f}(k) = \alpha_{i,f} m_{i,f}(k) + (1 - \alpha_{i,f}) m_i(k) \tag{1}$$

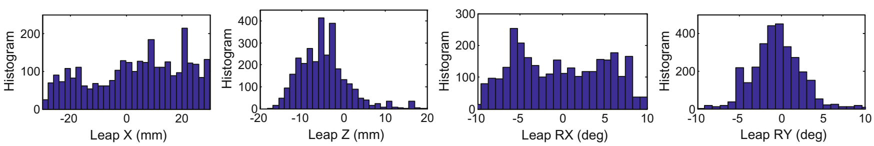

Fig. 5 Histograms for human adjustments in ten experiments

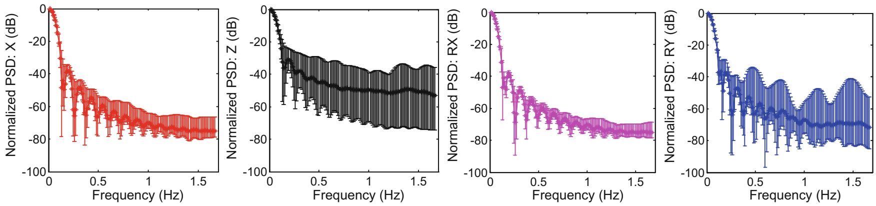

Fig. 6 Normalized PSDs for human adjustments in ten experiments

where $m_{i,f}(k), i = 1, \ldots, 4$ is the filtered movement for *X*, *Z*, *RX* and *RY* at instant *k*, $\alpha_{i,f}$ is the corresponding filtering coefficient, and $m_i(k)$ is the measured movement at instant *k*.

From Fig. 6 it is observed that different filtering coefficients should be applied for different movements. In this study $\alpha_{i,f} = [0.1, 0.7, 0.15, 0.5]$, selected based on each movement's PSD variances ($\mathrm{var(PSD}_i) = [19.2, 98.6, 11.9, 67.5]$). In the next section, teleoperated training experiments are conducted where the filtered human motion is tracked by the welding robot, and the experimental data are presented/analyzed.

3 Training Experiments and Data Analysis

3.1 Training Experiments

In the training experiments pipe welding is performed using the direct current electrode negative GTAW process. The welding position is 5G (i.e., the pipe stays stationary during welding, and the welding torch moves along the weld joint). The material of the pipe is stainless steel 304. The outer diameter and wall thickness of the pipe are 113.5 and 2.03 mm, respectively. Seven training experiments are performed by a human welder to model the correlation between the weld pool characteristic parameters (weld pool width, length, and convexity) and human hand movements. In these experiments the welding current is randomly changed from 40 to 48 A resulting in a fluctuating weld pool surface. The welder adjusts the movement based on the weld pool image feedback; the adjustments (*X*, *Z*, *RX*, and *RY*) are measured by leap sensor, filtered using Eq. (1), and sent to the robot. The robot follows the welder's movement and completes the welding task. Other experimental parameters are detailed in Table 1. Three weld pool characteristic parameters are selected as the system inputs, which are considered as the major sources a human welder perceives to complete the welding tasks. Four human welder movements are the system outputs. The sampling frequency in this study is 3 Hz because the welder controls the torch movement by observing the weld pool and is thus a relatively slow process.

Table 1 Experiment parameters

Welding parameters				
Current/A	Welding speed/mm/s	Arc length/mm	Torch orientations/°	Argon flow rate/L/min
40–48	–	–	–	11.8
Monitoring parameters				
Project angle/°	Laser to weld pool distance/mm		Imaging plane to weld pool distance/mm	
31.5	24.7		101	
Camera parameters				
Shutter speed/ms	Frame rate/fps		Camera to imaging plane distance/mm	
2	10		57.8	

Figure 7 shows the robot tracking performance in a sample training experiment, and Fig. 8 depicts the front-side and back-side weld bead in this experiment. Acceptable tracking performance is achieved in all four movements. It is noted, however, that certain human hand movements are not perfectly tracked, especially in *RX* and *RY*. Accurate tracking performance is challenging when the human makes large movement, which will be authors' future research.

Figure 9 plots the welder's movement adjustments, and weld pool characteristic parameters (weld pool width, length, and convexity) in seven training experiments. As can be observed, the human welder manipulates the virtual welding torch accordingly based on the weld pool geometry he/she perceives. In the next subsection, data analysis is performed and the importance of each movement is compared, which will be utilized to construct the welder rating system in Sect. 4.

3.2 Data Analysis

To evaluate each human hand movement's impact on the weld pool characteristic parameters and consequent weld penetration (characterized by its back-side bead width), linear modeling is conducted. The following first order Auto Regression Moving Average (ARMA) model is proposed:

$$\begin{cases} W_k = a_W W_{k-1} + \sum_{j=1}^{4} b_{W,j} u_{j,k-1} + c_W \\ L_k = a_L L_{k-1} + \sum_{j=1}^{4} b_{L,j} u_{j,k-1} + c_L \\ C_k = a_C C_{k-1} + \sum_{j=1}^{4} b_{C,j} u_{j,k-1} + c_C \end{cases} \quad (2)$$

where W_k, L_k, C_k are the weld pool width, length, and convexity at instant k. $u_{j,k-1}, j = 1, \ldots, 4$ are the welding speed S, arc length A (relative to 4 mm), rotation adjustment along welding direction RX(relative to the normal of the pipe surface), and rotation perpendicular to the welding direction RY, respectively. a, b, c

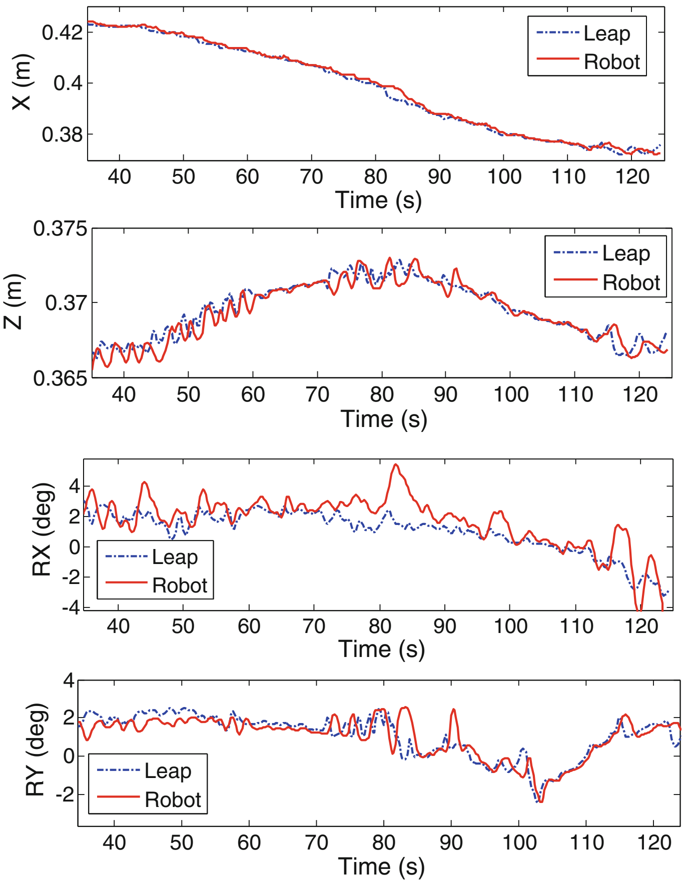

Fig. 7 Robot tracking performance in a sample teleoperation learning experiment

Fig. 8 Front-side (**a**) and back-side (**b**) weld bead in the sample teleoperation learning experiment in Fig. 7

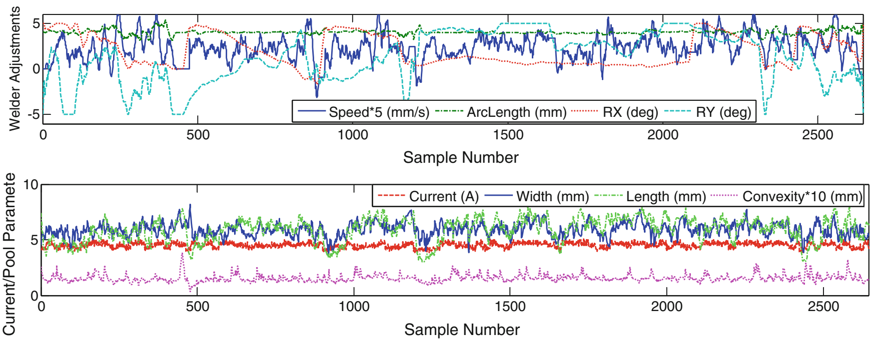

Fig. 9 Measured welder adjustments and pool parameters in seven teleoperated training experiments

are the model parameters associated with each model. These parameters can be identified using standard least squares method. The identified models are:

$$\begin{cases} W_k = 0.3W_{k-1} + 0.04S_{k-1} + 0.05A_{k-1} - 0.04RX_{k-1} + 0.01RY_{k-1} + 4.2 \\ L_k = 0.6L_{k-1} + 0.2S_{k-1} + 0.08A_{k-1} - 0.08RX_{k-1} + 0.03RY_{k-1} + 2.6 \\ C_k = 0.01C_{k-1} - 0.06S_{k-1} + 0.04A_{k-1} + 0.004(RX_{k-1} + RY_{k-1}) + 0.4 \end{cases} \tag{3}$$

The corresponding steady state models are:

$$\begin{cases} W_s = 0.059S_s + 0.066A_s - 0.053RX_s + 0.008RY_s + 5.99 \\ L_s = 0.56S_s + 0.18A_s - 0.18RX_s + 0.06RY_s + 5.93 \\ C_s = -0.059S_s + 0.042A_s + 0.004(RX_s + RY_s) + 0.42 \end{cases} \tag{4}$$

Based on authors' previous study [27], the following steady state model between the back-side bead width and pool parameters can be expressed as:

$$Wb_s = 0.9W_s - 0.45L_s + 1.27C_s + 1.7 \tag{5}$$

where Wb_s is the back-side bead width in steady-state.

Substituting Eqs. (4) in (5), we have:

$$Wb_s = -0.27S_s + 0.03A_s + 0.04RX_s - 0.01RY_s + 4.96 \tag{6}$$

This steady-state correlation indicates that when the welding speed increases, the back-side bead width decreases. This makes sense because an increase in the welding speed decreases the heat input into the process and the penetration is thus reduced. Comparing the impact between four welder movements, it is observed that the welding speed, arc length, rotations along and perpendicular to the welding direction contribute to the back-side bead width with percentages of [76.4, 8.6, 11, 4%], respectively. It is thus concluded that the welding speed adjustment has dominant contribution to the weld penetration, but welder adjustment in arc length and torch orientations also contribute to the weld penetration to some extent. In the next section, the normalized coefficients (i.e., [0.764, 0.086, 0.11, 0.04]) will be utilized to form the welder rating system.

4 Welder Rating System

Because the limit of the welder's skill, the real-time adjustments depicted in Fig. 9 might contain certain amount of "bad operation". However, only "good response" should be utilized to form the human response model. In this section, a welder rating system is constructed, and "good response" is selected as the data pairs for the human response modeling process detailed in Sect. 5. As a preparation, Neuro-fuzzy and ANFIS modeling technique is briefly reviewed, which will then be utilized in forming the welder rating system and human response model.

4.1 Neuro-Fuzzy and ANFIS Modeling

Neuro-fuzzy approach (i.e., the fusion of the NNs and fuzzy logic) determines the parameters in fuzzy models using learning techniques developed in neural networks [28], and has been successfully applied in various areas [13–15, 29–31]. Jang [29] developed ANFIS by using a hybrid learning procedure. It possesses the advantages of adaptive rule changing capability, fast convergence rate, and does not require extensive experiences about the process to construct the fuzzy rules. A typical fuzzy rule in a Sugeno-type model has the form [28]:

$$\text{IF}\, x\, \text{is}\, A\, \text{and}\, y\, \text{is}\, B, \quad \text{then}\, z = f(x,\ y) \tag{7}$$

where A and B are fuzzy sets, and $z = f(x, y)$ is a linear function.

ANFIS can construct an input–output mapping in the form of Sugeno type if-then rules by using a hybrid learning procedure [29]. A fuzzy logic control/decision network is constructed automatically by learning from the training data. The membership function (MF) adopted in this study is generalized bell MF specified by three parameters [27]:

$$A_{ji}(p_j; a_{ji}, b_{ji}, c_{ji}) = \frac{1}{1 + \left|\left(p_j - c_{ji}\right)/a_{ji}\right|^{2b_{ji}}} \tag{8}$$

where p_j is the fuzzy variables and a_{ji}, b_{ji}, c_{ji} are the input fuzzy membership function parameters.

For a given set of input variables (for example p_1, p_2, and p_3), the following rule is implemented [29]:

$$\text{Rule } (i_1, i_2, i_3) : \text{IF } p_1 \text{ is } \mathrm{A}_{1i1}, p_2 \text{ is } \mathrm{A}_{2i2}, \quad \text{and } p_3 \text{ is } A_{3i3},$$
$$\text{Then } y(i_1, i_2, i_3) = d_1(i_1, i_2, i_3)p_1 + d_2(i_1, i_2, i_3)p_2 + d_3(i_1, i_2, i_3)p_3 + d_0(i_1, i_2, i_3) \tag{9}$$

where d_j's are the consequent parameters.

The final output of the fuzzy model is [29]:

$$y = \sum_{i_1=1}^{2}\sum_{i_2=1}^{2}\sum_{i_3=1}^{2} w(i_1, i_2, i_3)y(i_1, i_2, i_3) \tag{10}$$

where $w(i_1, i_2, i_3)$ is the weight representing the truth degree for the premise: p_1 is A_{1i1}, p_2 is A_{2i2}, and p_3 is A_{3i3}, and is expressed by the following equation:

$$w(i_1, i_2, i_3) = \prod_{j=1}^{3} A_{ji_k}(p_j) \tag{11}$$

The output Eq. (10) together with the weighting Eq. (11), membership function (8), and the fuzzy rule (9) form an ANFIS model. Its model parameters a_{ji}, b_{ji}, c_{ji} and d_j's can be identified using the Matlab ANFIS toolbox.

The following two criteria are proposed to evaluate the performance of the linear and ANFIS models. The model average error is defined as:

$$E_{ave} = \frac{1}{n}\sum_{k=1}^{n} |\hat{y}_k - y_k|, (k = 1, \ldots, n) \tag{12}$$

where n is the number of data points, y_k is the measurement at instant k, and $\hat{y}_k$ is the model estimation.

The root mean square error (RMSE) is calculated by:

$$RMSE = \sqrt{\sum_{k=1}^{n} (\hat{y}_k - y_k)^2 / n} \tag{13}$$

4.2 Automated Welder Rating System

To better distill the correct response of the human welder, the human welder evaluates the measured data (including the welding current, weld pool characteristic parameters) and corresponding back-side weld penetration, then assigns a rating (from 0 to 10) in each 5 s interval. (Assigning a rating is an off-line process requiring no real-time operation/control and is thus much less skill demanding for the welder.) Figure 10 shows the assigned rating and Fig. 12 plots its histogram.

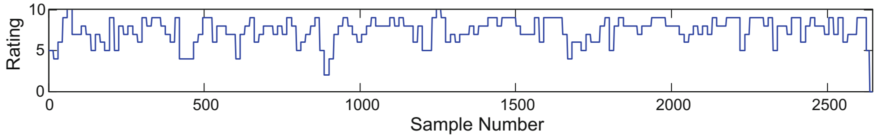

Fig. 10 Human welder rating in seven dynamic training experiments

It is seen that over 60% of the data points are rated above 8, however about 10% of the data points have been rated below 4. If all the data points are used to model the human welder response, the model might not reflect the correct behavior. In this section, an ANFIS based automated welder rating system (i.e., classifier) is synthesized.

From steady state models derived in Sect. 3.2 it is observed that each welder adjustment has certain impact on the weld penetration and thus should be accordingly weighted. The individual welder rating systems corresponding to each input are defined as:

$$\begin{cases} R_{S,k} = f_1(W_k, L_k, C_k, S_k) \\ R_{A,k} = f_2(W_k, L_k, C_k, A_k) \\ R_{RX,k} = f_3(W_k, L_k, C_k, RX_k) \\ R_{RY,k} = f_4(W_k, L_k, C_k, RY_k) \end{cases} \tag{14}$$

where W_k, L_k, C_k represent the measured weld pool parameters at instant k.

Then both the linear and ANFIS welder rating system can be synthesized by weighting the individual welder rating system for four inputs using the normalized coefficients derived in Sect. 3.2:

$$R_k = 0.764R_{S,k} + 0.086R_{A,k} + 0.11R_{RX,k} + 0.04R_{RY,k} \tag{15}$$

Linear model can be fitted using standard least squares method:

$$\begin{cases} R_{S,k} = 0.018W_k - 0.107L_k - 0.111C_k + 3.831S_k + 6.17 \\ R_{A,k} = -0.016W_k + 0.098L_k - 1.152C_k - 0.279A_k + 7.29 \\ R_{RX,k} = -0.012W_k + 0.163L_k - 1.678C_k + 0.102RX_k + 6.83 \\ R_{RY,k} = -0.006W_k + 0.009L_k - 1.149C_k + 0.124RY_k + 7.59 \end{cases} \tag{16}$$

The linear fitting result is depicted in Fig. 11. Substantial fitting errors are frequently observed. The model average error and RMSE are 0.876 and 1.112, respectively.

ANFIS modeling technique described in previous subsection is then utilized to improve the classifier performance. Modeling trials suggest that when the four inputs are partitioned by 2, a good trade-off between fitting errors and model parameter numbers is obtained. ANFIS fitting result is also plotted in Fig. 12. Compared to the linear model result, the proposed ANFIS model provides much

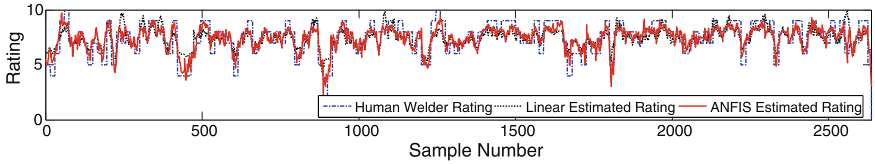

Fig. 11 Human welder rating, linear and ANFIS estimated rating in seven dynamic training experiments

Fig. 12 Histogram of the human welder rating specified in Fig. 10

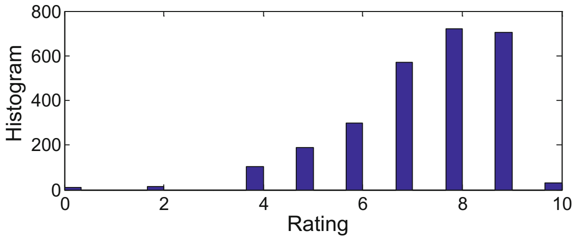

better fitting result with the model average error and RMSE being reduced to 0.692 and 0.878, respectively.

The trained classifier will be used to classify the training experiment data (shown in Fig. 9). Measurements (with associated ratings larger than 8) are then selected and depicted in Fig. 13. These measurements are considered to be the “correct response” generated by the human welder. In the next section, modeling of human welder response is conducted and correct human welder response is distilled and analyzed. The proposed classifier can also be used in the welder training systems to rate welder adjustments, which may be helpful in training unskilled welder faster, and resolve the skilled welder shortage issue in the manufacturing industry.

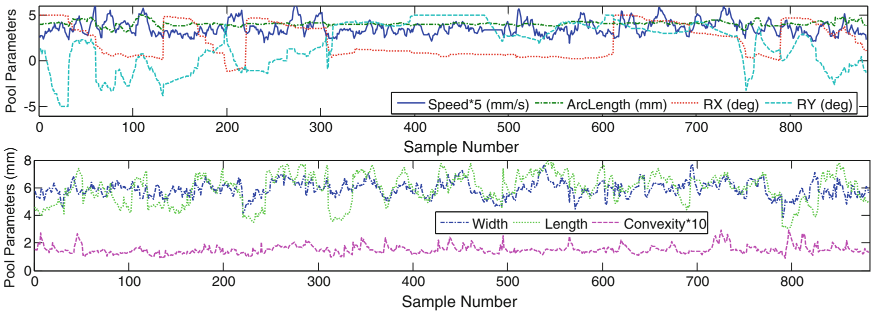

Fig. 13 Selected data pairs (measurements with ratings larger than 8) from Fig. 9

5 Data-Driven Modeling of 3-D Human Hand Movement

Based on the definition of system inputs and output detailed in previous section, a general model structured is described as:

$$\begin{cases} S_k = g_1(W_{k-1}, L_{k-1}, C_{k-1}) \\ A_k = g_2(W_{k-1}, L_{k-1}, C_{k-1}) \\ RX_k = g_3(W_{k-1}, L_{k-1}, C_{k-1}) \\ RY_k = g_4(W_{k-1}, L_{k-1}, C_{k-1}) \end{cases} \tag{17}$$

In the next two subsections, linear and ANFIS modeling are performed to correlate the weld pool characteristic parameters to the welder adjustments.

5.1 Linear Modeling

The following linear models are first proposed and identified using standard least squares algorithm:

$$\begin{cases} S_{k,l} = 0.0014W_{k-1} + 0.0278L_{k-1} + 0.2322C_{k-1} + 0.4551 \\ A_{k,l} = -0.0352W_{k-1} + 0.028L_{k-1} + 0.683C_{k-1} - 0.123 \\ RX_{k,l} = -0.0445W_{k-1} - 0.597L_{k-1} + 6.558C_{k-1} + 3.961 \\ RY_{k,l} = 0.0631W_{k-1} + 0.646L_{k-1} + 3.595C_{k-1} - 3.592 \end{cases} \tag{18}$$

The linear modeling results are plotted in Fig. 14. The average model errors and RMSEs are listed in Table 2. It is found that the human movements can be estimated by the linear model with acceptable accuracy. However, substantial static fitting errors are frequently observed.

5.2 ANFIS Modeling

The linear model described in the first subsection accounts for the average effect of the weld pool parameters on the welder adjustments in the large input ranges. In order to further improve the modeling accuracy, nonlinear ANFIS modeling method is utilized. Modeling trails suggest that when input parameters are partitioned by 2, a good trade-off is obtained between model performance and number of model parameters. The modeling result is shown in Fig. 14 and the resulting ANFIS model errors are listed in Table 2. It is seen that the model errors are improved by incorporating the nonlinear correlation between the model inputs and outputs. Hence, the developed ANFIS modeling plays an important role in deriving the detailed correlation between the welder's response and the weld pool geometry.

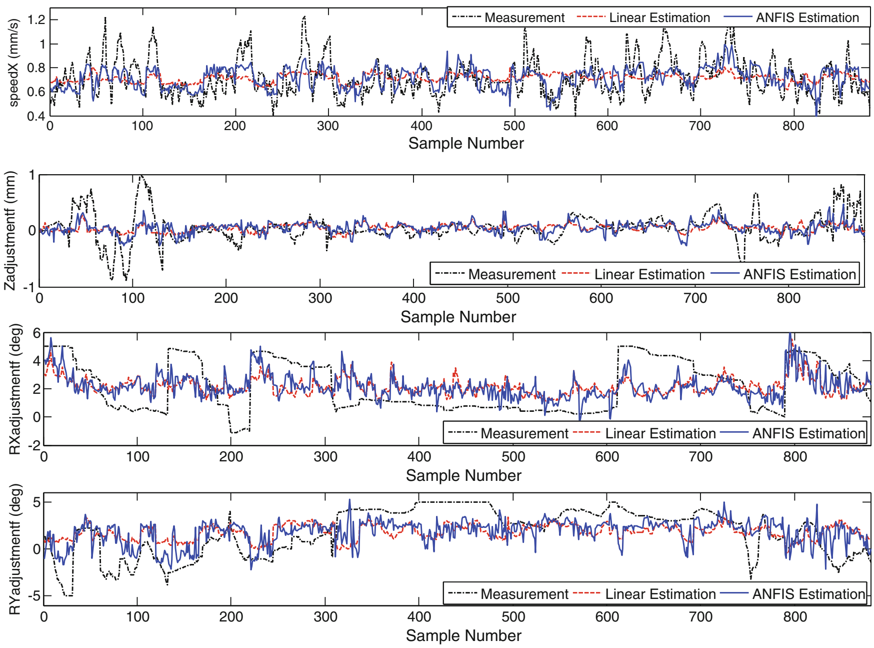

Fig. 14 Modeling results of human welder adjustments

Table 2 Model error comparisons

		Average model error	RMSE
S (mm/s)	Linear	0.121	0.152
	ANFIS	0.102	0.129
A (mm)	Linear	0.167	0.245
	ANFIS	0.158	0.232
RX (deg)	Linear	1.524	1.685
	ANFIS	1.356	1.571
RY (deg)	Linear	1.981	2.352
	ANFIS	1.717	2.122

Figure 15 plots the histogram of the rating for data specified in Fig. 13. It is observed that after ANFIS modeling, the overall rating is increased, with more ratings above 8.4, and less ratings from 8 to 8.4. This indicates that the proposed ANFIS modeling is able to distill the correct response made by the human welder.

Fig. 15 Histogram of the human welder ratings calculated from data pairs specified in Fig. 13

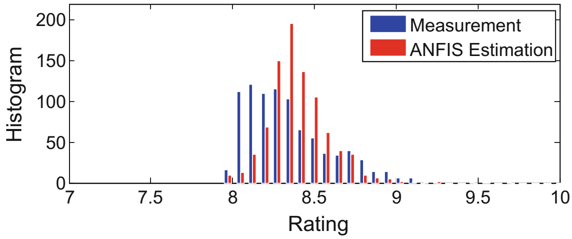

5.3 *Model Verification*

To verify the proposed ANFIS model, verification experiment is conducted and the results are shown in Fig. 16. It is shown in Fig. 16b that the model can estimate the welder adjustments with acceptable accuracy. It is noticed, however, that certain human adjustments are not learned by the models. Careful analysis indicates that these adjustments are caused by human welder's underestimation and overestimation of the weld penetration, and thus should not be learned.

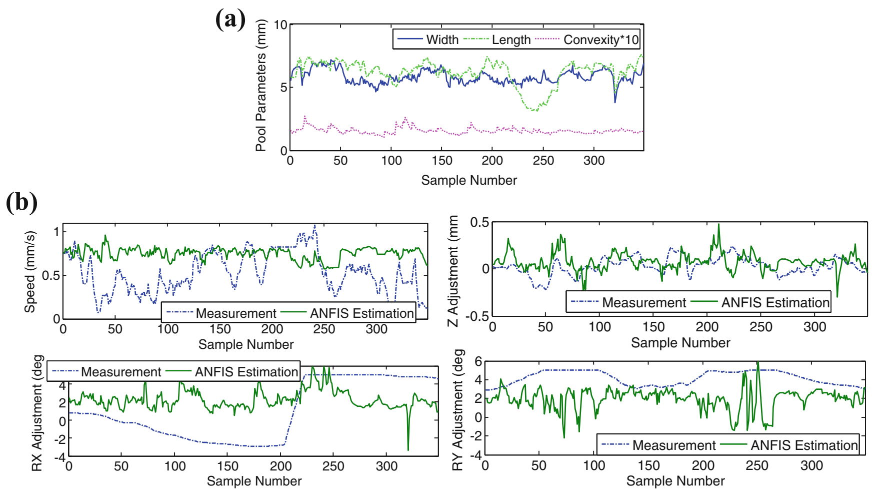

Fig. 16 Verification experiment results: **a** weld pool characteristic parameters; **b** measured and estimated welder adjustments

6 Automated Welding Experiments

In order to demonstrate the robustness of the developed control system, automated welding experiments have been designed and conducted in this section under different disturbances. In subsection 6.1, different welding currents are applied. In subsection 6.2 and 6.3 the welding speed and weld pool measurement disturbances are applied and the robustness of the controller with speed disturbance is tested.

6.1 Experiment 1: Different Welding Currents

In this subsection the control experiment is conducted under different welding currents. From 40 s to 50 s is the open loop period where no controller is applied. The welding speed and the welding current are set at 0.5 mm/s and 43 A, and other adjustments are set at zeros. The pool parameters reach their steady states at the end of the open loop period (6 mm for the width, 6 mm for the length, and 0.13 mm for the convexity). From 50 s the proposed controller is applied, and the welding speed is adjusted to about 0.7 mm/s based on the inputs (weld pool characteristic parameters). Other welding parameters including the arc length and torch orientations are adjusted accordingly. It is noticed that for the same welding current (i.e., 43 A), the weld pool parameters are fluctuating because of other un-modeled factors that might influence the welding process. For example, from 75 s to 80 s, an increase in the weld pool convexity is observed. Consequently, the welding speed is increased, the arc length is slightly decreased, and the orientations are also adjusted accordingly to compensate this change in the weld pool parameters, similar to the adjustments that would be made by the human welders.

At 95 s, the welding current is changed to 46 A (Fig. 17a). As a result, the weld pool width, length and convexity gradually increase to about 6.5, 7, and 0.14 mm, respectively. From Fig. 17 d it is also observed that the back-side bead width is increased because of this current increase. If no closed loop control is applied, this current increase cannot be compensated. From Fig. 17b it is shown that the controller is able to increase the welding speed to about 0.8 mm/s to compensate this increase in the welding current. The back-side bead width is also well maintained at about 2 mm.

6.2 Experiment 2: Welding Speed Disturbance

In this experiment the robustness of the control algorithm against welding speed disturbance is evaluated. The welding current is set at 43 A throughout the experiment. An artificial error between the calculated and applied values of the welding speed is applied. In the first 35 s of the closed loop control (60 s–95 s), no error exists between

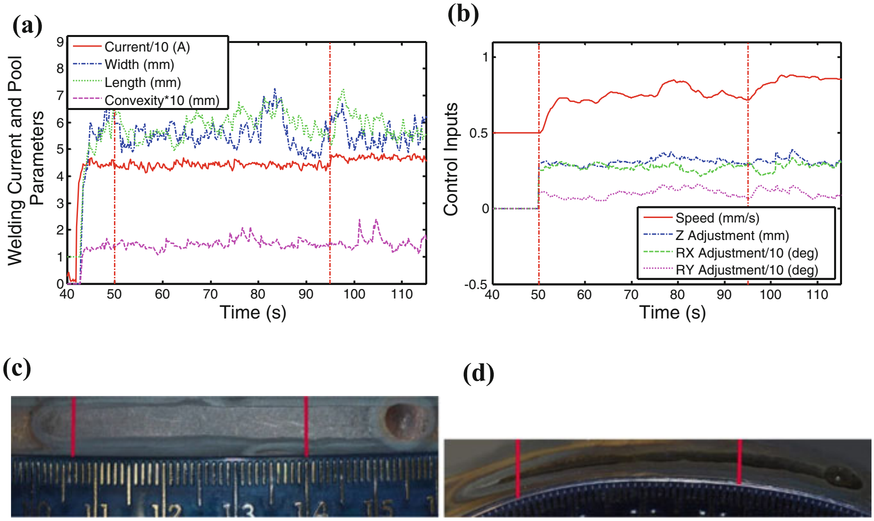

Fig. 17 Experiment 1 results: **a** welding current and weld pool parameters; **b** control inputs; **c** front-side bead; **d** back-side bead

the calculated speed and applied speed. The controller is able to bring the back-side bead width to about 2.1 mm. From 95 s to 97 s, the welding speed is set at 0.5 mm/s. As the result, the back-side bead width increases to about 2.5 mm (see Fig. 18d). However, the controller is able to adjust the welding speed to compensate this artificial error (see Fig. 18c), and the back-side bead width can be maintained around 2.1 mm again (see Fig. 18d) with a relatively quick response time.

6.3 *Experiment 3: Measurement Disturbance*

An artificial error between the actual and measured values of the weld pool surface is applied in this experiment. At 113 s, the measured weld pool width, length, and convexity are set to 3, 3.5, and 0.05 mm, respectively. As can be seen from Fig. 19b the welding speed is slightly decreased from 0.8 mm/s to about 0.76 mm/s, and the back-side bead width is slightly increased (Fig. 19d). Other welding parameters are also adjusted by the controller accordingly. By applying the controller, the desired back-side bead width is well maintained at about 2.1 mm. The robustness of the proposed intelligent controller is thus demonstrated.

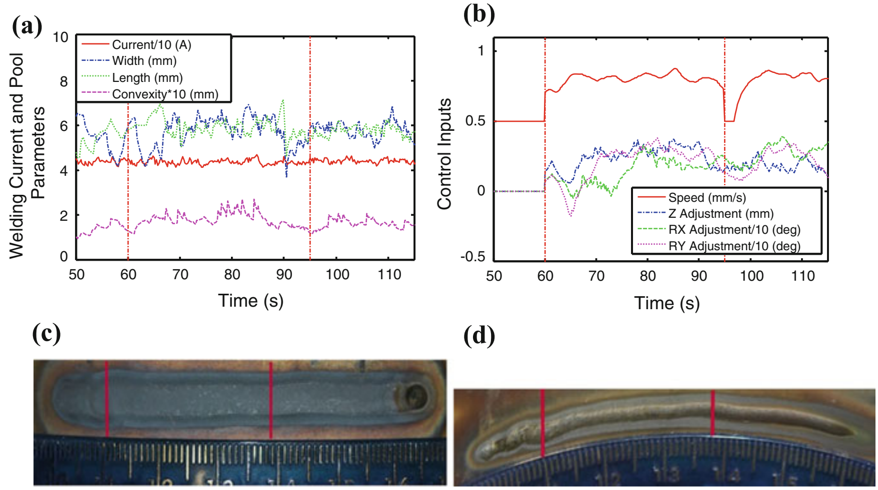

Fig. 18 Experiment 2 results: **a** welding current and weld pool parameters; **b** control inputs; **c** front-side bead; **d** back-side bead

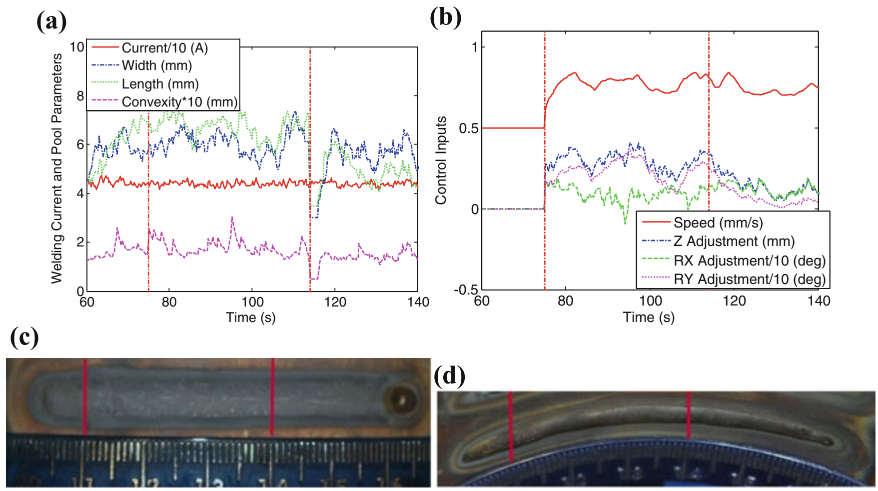

Fig. 19 Experiment 3 results: **a** welding current and weld pool parameters; **b** control inputs; **c** front-side bead; **d** back-side bead

7 Conclusion

In this paper a data-driven approach to model human welder intelligence in 3-D is proposed. A virtualized welding platform is utilized to conduct teleoperated training experiments. Human welder's arm gestures (including movement speed, arc length, and torch orientations) together with the 3-D weld pool characteristic parameters are recorded and analyzed. The data is off-line rated by the welder and an automated welder rating system is obtained by synthesizing individual rating system corresponding to each welder adjustment using weights from their steady state models. Data from the training experiments are then selected and ANFIS models are proposed to correlate the 3-D weld pool characteristic parameters and welder's movement adjustments. To demonstrate the effectiveness of the proposed data-driven model, automated control experiments are conducted. Results show that the proposed model as an intelligent controller is able to control the welding process under different welding currents, and is robust against welding speed and measurement disturbances. A foundation is thus established to rapidly extract human intelligence and transfer such intelligence into welding robots.

Future work includes achieving more accurate tracking performance of the torch movement, as well as detailed analysis of the interactions and coupling between welding speed and torch orientations. Other interesting applications can also be explored, such as speeding up the welder training process. The response models learned from unskilled welders being trained can be compared with those from skilled welders to further understand their differences.

Acknowledgements This work is funded by the National Science Foundation (IIS-1208420). The authors thank the assistance from Mr. Ning Huang on the experiments.

References

1. O'Brien R (ed) (1998) Welding handbook, vol 2, 8th edn. Welding Processes, AWS, Miami FL
2. Renwick R, Richardson R (1983) Experimental investigation of GTA weld pool oscillations. Weld J 62(2):29s–35s
3. Matsui H, Chiba T, Yamazaki K (2014) Detection and amplification of the molten pool natural oscillation in consumable electrode arc welding. Weld Int 28(1):5–12
4. Carlson N, Johnson J (1988) Ultrasonic sensing of weld pool penetration. Weld J 67(11): 239s–246s
5. Guu AC, Rokhlin SI (1992) Arc weld process control using radiographic sensing. Mater Eval 50(11):1344
6. Song JB, Hardt DE (1993) Closed-loop control of weld pool depth using a thermally based depth estimator. W J 72(10):471s–478s
7. Pietrzak KA, Packer SM (1994) Vision-based weld pool width control. J Eng Ind Trans ASME 116(1):86–92
8. Chen H, Lv F, Lin T et al (2009) Closed-loop control of robotic arc welding system with full-penetration monitoring. J Intell Rob Syst 56(5):565–578

9. Liu YK, Zhang YM (2013) Model-based predictive control of weld penetration in gas tungsten arc welding. IEEE Trans Control Syst Technol 22(3):955–966
10. Liu YK, Zhang YM (2013) Control of 3D weld pool surface. Control Eng Pract 21(11):1469–1480
11. Zhang WJ, Liu YK, Wang X, Zhang YM (2012) Characterization of three dimensional weld pool surface in GTAW. Weld J 91(7):195s–203s
12. Liu YK, Zhang WJ, Zhang YM (2015) Nonlinear modeling for 3d weld pool characteristic parameters in GTAW. Weld J 94:231s–240s
13. Liu YK, Zhang WJ, Zhang YM (2015) Dynamic neuro-fuzzy based human intelligence modeling and control in GTAW. IEEE Trans Autom Sci Eng 12(1):324–335
14. Liu YK, Zhang YM, Kvidahl L (2014) Skilled human welder intelligence modeling and control: part I—modeling. Weld J 93:46s–52s
15. Liu YK, Zhang YM, Kvidahl L (2014) Skilled human welder intelligence modeling and control: part II—analysis and control applications. Weld J 93:162s–170s
16. Uttrachi GD (2007) Welder shortage requires new thinking. Weld J 86(1):6
17. Cary HB, Helzer SC (2005) Modern welding technology. Pearson/Prentice Hall
18. Liu YK, Zhang YM (2014) Control of human arm movement in machine-human cooperative welding process. Control Eng Pract 32:161–171
19. Liu YK, Zhang YM (2015) Controlling 3d weld pool surface by adjusting welding speed. Weld J 94:125s–134s
20. Liu YK, Zhang YM (2015) Iterative local anfis based human welder intelligence modeling and control in pipe GTAW process: a data-driven approach. IEEE/ASME Trans Mechatron 20 (3):1079–1088
21. Liu YK, Zhang YM (2017) Supervised learning of human welder behaviors for intelligent robotic welding. IEEE Trans Autom Sci Eng 14(3):1532–1541
22. Liu YK, Zhang YM (2017) Fusing machine algorithm with welder intelligence for adaptive welding robots. J Manuf Processes 27:18–25
23. Liu YK (2016) Toward intelligent welding robots: virtualized welding based learning of human welder behaviors. Weld World 60(4):719–729
24. Liu YK, Shao Z, Zhang YM (2014) Learning human welder movement in pipe GTAW: a virtualized welding approach. Weld J 93:388s–398s
25. Liu YK, Zhang YM (2015) Toward welding robot with human knowledge: a remotely-controlled approach. IEEE Trans Autom Sci Eng 12(2):769–774
26. Daniel T (2012) Leap motion: 3D hands-free motion control, unbound, http://news.cnet.com/8301-11386_3-57437404-76/leap-motion-3d-hands-free-motion-control-unbound/ Accessed 20 May 2012
27. Liu YK, Zhang WJ, Zhang YM (2013) Estimation of weld joint penetration under varying GTA pools. Weld J 92(11):313s–321s
28. Tanaka K, Sano M, Watanabe H (1995) Modeling and control of carbon monoxide concentration using a neuro-fuzzy technique. IEEE Trans Fuzzy Syst 3(3):271–279
29. Jang JSR (1993) ANFIS: Adaptive-network-based fuzzy inference systems. IEEE Trans Syst Man Cybern 23(3):665–685
30. Zhao L et al (2014) Data-based modeling of vehicle crash using adaptive neural-fuzzy inference system. IEEE/ASME Trans Mechatron 19(2):684–696
31. Druitt CM, Alici G (2014) Intelligent control of electroactive polymer actuators based on fuzzy and neurofuzzy methodologies. IEEE/ASME Trans Mechatron 19(6):1951–1962